High Contrast Imaging with the New Vortex Coronagraph on NACO

Dimitri Mawet[1]
Olivier Absil[2]
Julien H. Girard[1]
Julien Milli[1,3]
Jared O'Neal[1]
Christian Delacroix[2]
Pierre Baudoz[4]
Anthony Boccaletti[4]
Pierre Bourget[1]
Valentin Christiaens[2]
Pontus Forsberg[5]
Frederic Gonté[1]
Serge Habraken[1]
Charles Hanot[2]
Mikael Karlsson[5]
Markus Kasper[1]
Anne-Marie Lagrange[3]
Jean-Louis Lizon[1]
Koraljka Muzic[1]
Eduardo Peña[1]
Richard Olivier[6]
Nicolas Slusarenko[1]
Lowell E. Tacconi-Garman[1]
Jean Surdej[2]

[1] ESO
[2] Département d'Astrophysique, Géophysique et Océanographie, Université de Liège, Belgium
[3] Institut de Planétologie et d'Astrophysique de Grenoble (IPAG), Université Joseph Fourier, Grenoble, France
[4] LESIA, Observatoire de Paris, Meudon, France
[5] Department of Engineering Sciences, Ångström Laboratory, Uppsala University, Sweden
[6] GDTech s.a., Liège Science Park, Belgium

The installation and successful commissioning of an *L'*-band annular groove phase mask (AGPM) coronagraph on VLT/NACO is presented. The AGPM is a vector vortex coronagraph made from diamond sub-wavelength gratings tuned to the *L'*-band. The vector vortex coronagraph enables high-contrast imaging at very small inner working angles (here 0.09 arcseconds, the diffraction limit of the VLT at *L'*), potentially opening up a new parameter space in high-resolution imaging. During technical and science verification runs, we discovered a late-type companion at two beamwidths from an F0V star, and imaged the inner regions of β Pictoris down to the previously unexplored projected radius of 1.75 astronomical units. The circumstellar disc of β Pic was also resolved from 1 to 5 arcseconds. These results showcase the potential of the NACO *L'*-band AGPM over a wide range of spatial scales.

Introduction

High contrast imaging is an attractive technique to search for exoplanets as it provides a straightforward means to characterise them and their host systems through, e.g., orbital motion, spectrophotometry of the planetary atmospheres or planet–disc interactions. For these reasons, it constitutes one of the main science drivers of today's ground-based near-infrared adaptive optics instruments. One in two proposals to use NACO, VLT's adaptive optics workhorse instrument, is related to extrasolar system science. The same ratio is observed in the number of publications (see Figure 1).

In terms of the detection of new objects, the current capabilities of NACO have almost been exhausted, a situation faced by most first generation adaptive optics imagers and even the Hubble Space Telescope. This does not mean that new discoveries will come to a halt, but we seem to have reached a plateau simply because the current parameter space has been combed through pretty thoroughly (although it should be emphasised that the early surveys were not optimal and could be productively repeated). Recently, only a few objects have been discovered, and many non-detections reported and statistically interpreted (e.g., Chauvin et al., 2010; Vigan et al., 2012). The field is now in need of a technological breakthrough. It is expected that opening the parameter space to fainter/smaller planets closer to their parent stars will indeed bring many new objects (Crepp & Johnson, 2011). This intermediate parameter space will be opened by the second generation coronagraphic instruments that have started to arrive at all major observatories: SPHERE at the VLT (Beuzit et al., 2010); the Gemini Planet Imager (Macintosh et al., 2012); P3k-P1640 at Palomar (Oppenheimer et al., 2012); and SCExAO at Subaru (Martinache et al., 2012).

These new instruments have all been designed around coronagraphs fed by extreme adaptive optics systems, a configuration which is expected to break through the current contrast and inner working angle (IWA) floor. However, first generation instruments, such as NACO, still possess untapped potential that, only after ten years of operations and understanding, allow us to fully exploit it (Girard et al., 2012), especially in the mid-infrared (*L'*-band, from 3.5 to 4.2 μm). This wavelength range offers significant advantages compared to shorter wavelengths (Kasper et al., 2007): (i) the *L'*-band contrast of planetary-mass companions with

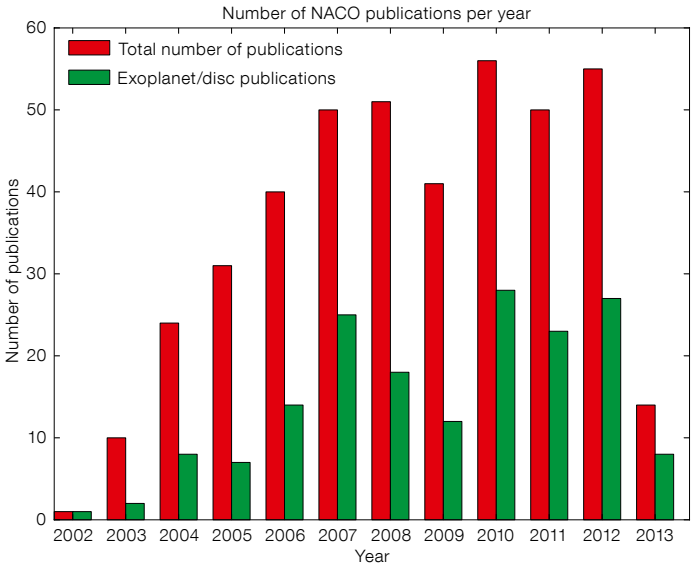

Figure 1. Total number of NACO refereed publications per year (red) and the number of articles related to extrasolar planetary system imaging and characterisation (green). Source: telbib[1].

respect to their host stars is predicted to be more favourable than in the *H*-band (e.g., Spiegel & Burrows, 2012) so that lower-mass, older objects can be addressed; and (ii) the *L′*-band provides better and more stable image quality, with Strehl ratios well above 70%, and sometimes as high as 90%, thus reducing speckle noise. These advantages certainly compensate for the increased sky background in the thermal infrared and the loss in resolution, especially if small IWA phase-mask coronagraphs are available.

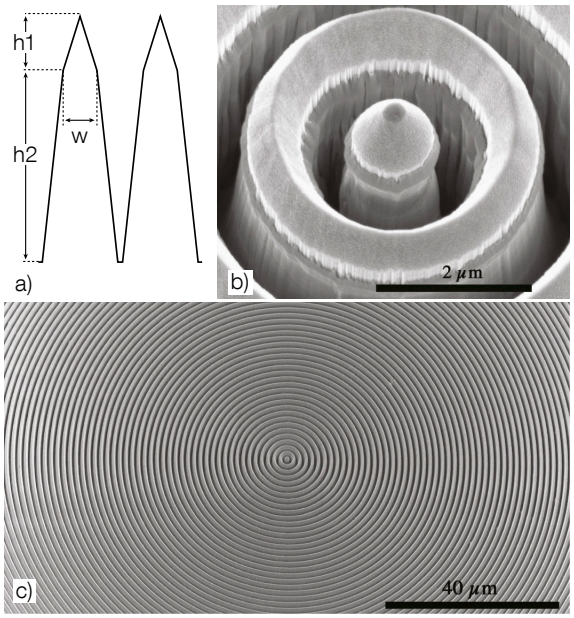

Figure 2. Scanning electron microscope images of the NACO AGPM made from diamond sub-wavelength gratings. a) The structure profile schematic, with h2 = 5 ± 0.1 μm, h1 = 1 ± 0.1 μm, and w = 0.65 ± 0.03 μm (the grating pitch is 1.42 μm). b) A zoom on the centre of the diamond AGPM. c) An overview of the structure showing the uniformity and original cleanliness of this particular device.

The annular groove phase mask vector vortex coronagraph

While working on the four-quadrant phase-mask (FQPM) coronagraph achromatisation for the future VLT-Planet Finder (SPHERE) more than ten years ago (work later published in Mawet et al. [2006]), the idea of making the FQPM circularly symmetric occurred (Mawet et al., 2005). It was quickly noticed that the FQPM is indeed nothing more than an overly discrete optical vortex. Optical vortices occur when the phase structure of light is affected by a helical ramp around the optical axis, given by $e^{il\theta}$, where θ is the focal plane azimuthal coordinate and l is the vortex "topological charge", i.e., the number of times the phase accumulates 2π along a closed path surrounding the phase singularity; i denotes $\sqrt{-1}$. The phase dislocation forces the amplitude to zero at its centre, which is a singularity. Nature prevents the phase from having an infinite number of values at a single point in space, which is non-physical, by simply nulling the light locally. In Mawet et al. (2005), we demonstrated for the first time that, when centred on the diffraction pattern of a star seen by a telescope, optical vortices have the remarkable property of affecting the subsequent propagation to the downstream Lyot stop by redirecting the on-axis starlight outside the pupil, where it is simply blocked.

On account of this property, and from the fact that it is a pure phase mask, the advantages of the vortex coronagraph over classical Lyot coronagraphs or phase/amplitude apodisers are: (i) small IWA, down to 0.9 λ/D, where λ is the wavelength of light and D the telescope diameter, e.g., 0.09 arcseconds in the *L′*-band at the VLT, thus slightly smaller than the diffraction limit; (ii) clear 360° off-axis field of view/discovery space; (iii) outer working angle set only by the instrument and/or mechanical/optical constraints; (iv) achromatic over the entire working waveband (here *L′*-band); (v) high throughput (here ~ 88%); and (vi) optical/operational simplicity.

Developed with colleagues and collaborators from the Université de Liege and the Observatoire de Paris-Meudon, we had no idea at the time that this concept would be potentially revolutionary and so difficult to realise. It took seven years to manufacture the first "vector vortex coronagraph" made from liquid crystal polymers at NASA-JPL (Mawet et al., 2009), and another three years to manufacture a fully functioning annular groove phase mask (AGPM) from diamond sub-wavelength gratings. The AGPM is one possible realisation of the vortex coronagraph, especially adapted to longer wavelengths (the first AGPM was actually optimised for the *N*-band, and installed in VISIR). It took two generations of PhD theses, the craftsmanship and the super high-tech capabilities of the Swedish foundry at Uppsala University to attain the stunning results presented here. The AGPM has now reached a sufficient readiness level for telescope implementation (Delacroix et al., 2013).

The AGPM selected for NACO was the third in a series of four realisations (AGPM-L3). Its theoretical raw null depth, limited by its intrinsic chromatism, was estimated (assuming a trapezoidal profile, see Figure 2) and measured to be around 5×10^{-3} (corresponding to a raw contrast of 2.5×10^{-5} at 2λ/D), which is more than needed for on-sky operations, where the limit is set by the residual wavefront aberrations.

The AGPM was installed inside NACO as part of a planned overhaul in November 2012. The AGPM was mounted on the entrance slit wheel by means of a dedicated aluminium mount, designed by GDTech s.a.. The mount was designed to sustain the differential contraction/dilatation of the aluminium relative to diamond, between room temperature and CONICA's working temperature of 60 K at the level of the slit/mask wheel, while providing enough thermal conduction capabilities. The assembly of the mount and AGPM was done on site at Paranal Observatory in a cleanroom environment (see Figure 3). Prior to on-sky tests and operations, a CONICA internal image of the mask was made (see Figure 4), revealing significant dust contamination, marginally affecting the background

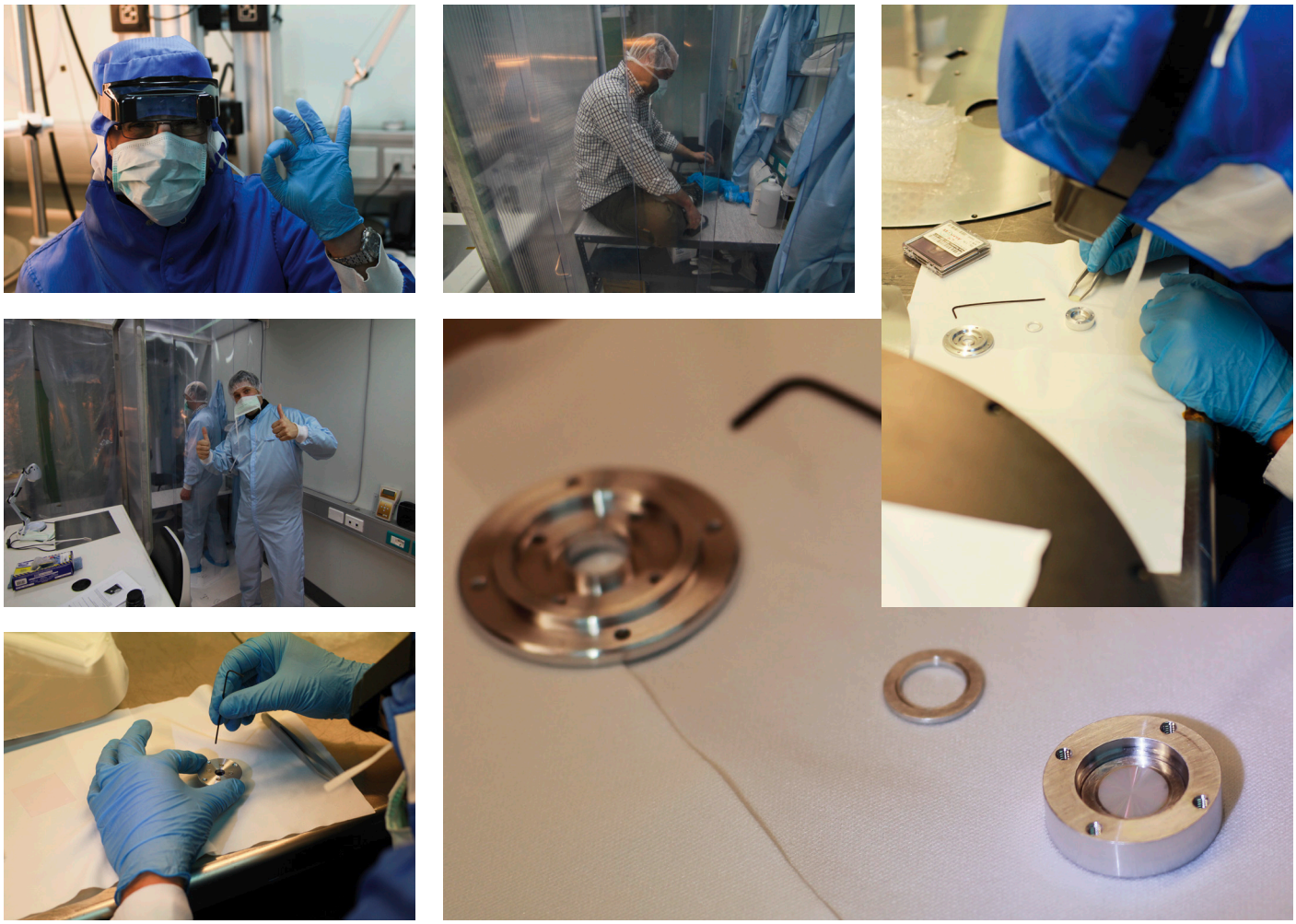

Figure 3 (above). Mounting of the AGPM in the Paranal cleanroom. The component, which looks like a tiny compact disc (10 mm diameter and 0.3 mm thickness), was handled with care and inserted into a dedicated mount (designed in Belgium by GDTech s.a. to support a cooldown from room temperature to a few tens of K). The assembly was then mounted onto the slit/mask wheel (focal plane) of CONICA. A great amount of synergy between Paranal Science Operations (Julien Girard and Dimitri Mawet, the Instrument Scientists) and Instrumentation (Jared O'Neal, the Instrument Responsible) was necessary for this whole process to succeed.

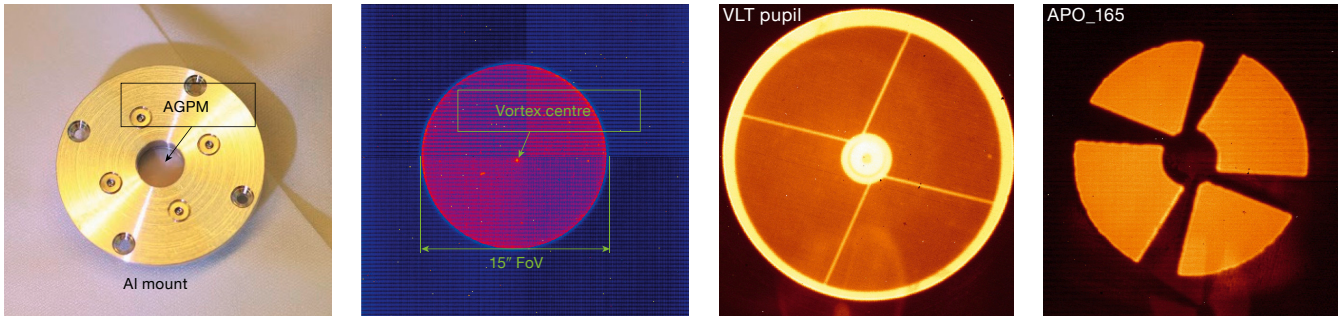

Figure 4 (below). From left to right: (i) The fully assembled aluminium mount with a 9 mm clear aperture containing the AGPM. (ii) View from inside CONICA, showing the 9 mm clear aperture corresponding to a 15-arcsecond field of view (diameter), fully contained within the 27-arcsecond field of view of CONICA's L27 objective. (iii) Full oversized stop of CONICA, showing the VLT pupil (including the central obscuration and struts). (iv) APO_165 pupil mask (diameter = 0.87 × D_{pupil}) available inside CONICA, aligned to cover the diffraction and thermal background from the central obscuration and struts.

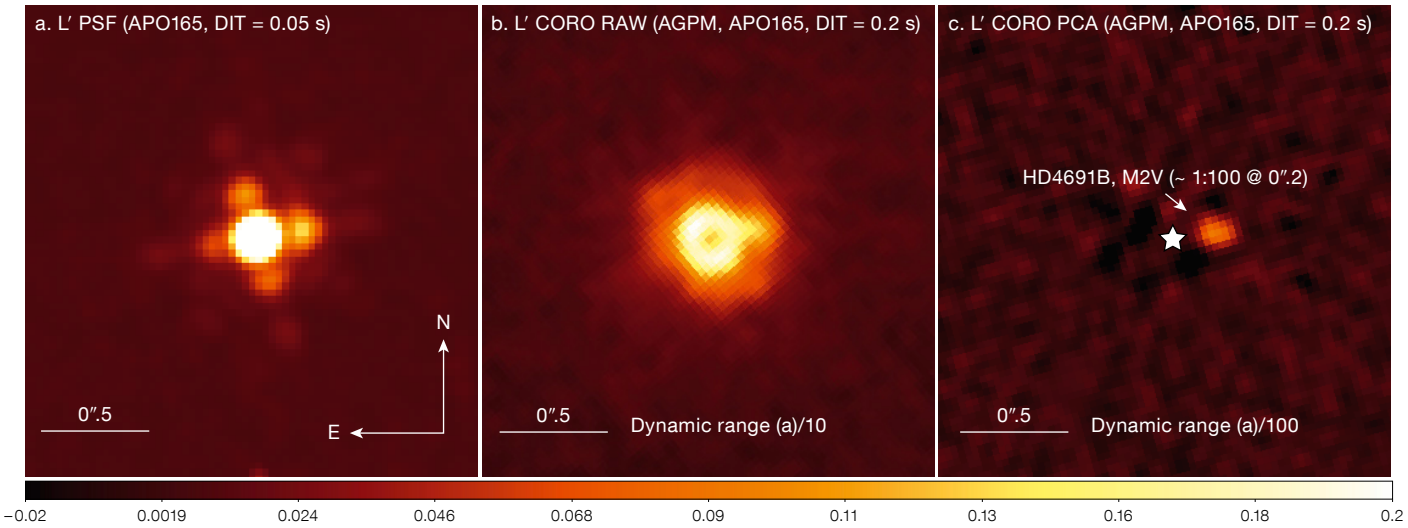

Figure 5. a) *L′*-band NACO PSF with the APO165 pupil mask in the beam. b) *L′*-band NACO coronagraphic image with the star centred on the AGPM (the dynamic range and corresponding colour bar scale are a factor of ten smaller than in image a). c) Result of our PCA-ADI data reduction pipeline, revealing a putative faint off-axis M2V companion at a separation of only ~ 0.19 arcsconds (the dynamic range and corresponding colour bar scale are a factor of 100 smaller than in image a). The scale is linear on all images (and scaled down by a factor of 10 and 100 for b and c, respectively), illustrating in sequence the benefits of coronagraphy and optimised data reduction technique. The bottom colour bar refers to Figure 5a.

noise. The slit wheel was set so that the centre of the AGPM falls close to, but slightly away from, CONICA's detector quadrant intersection. The AGPM field of view is ~ 15 arcseconds, corresponding to an outer working angle (OWA) of 7.5 arcseconds. The OWA is only limited by the size of the device (10 millimetres in diameter) and its mount. The mask transmittance at *L′*-band was measured on the sky to be 85 % ± 5 %, which is consistent with the theoretical value and laboratory measurements, both ~ 88 %, limited by imperfect antireflective treatments and mild absorption features around 4 µm (Delacroix et al., 2013).

In order to stabilise speckles, we used the pupil-tracking mode enabling angular differential imaging (ADI), which is perfectly adapted to the circular symmetry and 360° field of view of the AGPM. The CONICA camera is equipped with a pupil mask (APO_165) which blocks the telescope's central obscuration and spiders. Once correctly aligned with the pupil (in *x*, *y* and θ), this mask is optimal for use with the AGPM in pupil-tracking mode (see Figure 4). The measured throughput of the APO_165 mask used here is ~ 60 %. In terms of sensitivity, it is worth noting that the throughput loss is almost entirely compensated for by the improved thermal background. Indeed, the pupil obscuration is responsible for more than 25 % of the thermal emissivity of the telescope, even though its area only covers ~ 5 %. Blocking it with the APO_165 mask is therefore very efficient at reducing background noise, limiting the increase in background noise to 10 % with respect to non-coronographic imaging (Mawet et al., 2013).

First light: A discovery and breakthrough contrast capabilities

On 9 December 2012, a representative observing sequence was performed on the 1.9-Gyr-old main sequence standard star HD4691, under ~ 1.2 arcsecond visual seeing conditions. This star was chosen to maximise brightness and field rotation during the short time allocated for this technical test. A ~ 30-minute ADI sequence was obtained with a parallactic angle (PA) range of 30° and for a total exposure time of 200 seconds on source; the efficiency was mediocre for technical reasons. After acquiring an off-axis point spread function (PSF) star for photometric reference, we measured an instantaneous contrast of ~ 50 peak-to-peak (despite the average-to-bad conditions). The attenuation is about five times higher than measured with NACO's four-quadrant phase-mask coronagraph at *Ks* (Boccaletti et al., 2004). The coronagraph diffraction control yields two instantaneous benefits compared to classical imaging: (i) the peak saturation limit is decreased by a factor ~ 50; and (ii) the level of quasi-static speckles pinned to the PSF and the stellar photon noise limit are potentially decreased by a factor ~ 7, both within the AO control radius of 7λ/D. All in all, the *L′*-band AGPM coronagraph allows the background limit to be reached much closer in to the source.

After applying basic cosmetic treatment to our sequence of 100 frames (background subtraction, flat fielding and bad pixel/cosmic ray correction), we decided to use the quality and stability of the *L′*-band PSF provided by NACO to perform a sophisticated speckle subtraction. We used the very efficient principal component analysis (PCA) algorithm presented in Soummer et al. (2012). The result, using the whole image and retaining three main components, is presented in Figure 5. By pure chance, the object has a ~ 1 : 100 (or $\Delta L'$ ~ 5 mag) off-axis companion located at ~ 0.19 arcseconds (< 2λ/D), making this our first unexpected scientific result. The companion flux and astrometry were obtained by using the fake negative companion technique (Marois et al., 2010). At an absolute *L′*-band magnitude of 6.65, and age 1.9 Gyr for the system, the putative companion would most likely be an M2V star

at projected separation of 11.8 ± 0.4 astronomical units (AU), and 354.5 ± 0.6 degrees position angle (see Mawet et al. [2013] for more details).

Since the presence of the companion affects the contrast, we took another similar representative ADI sequence on a different standard star (HD123888). This technical test was performed under better conditions (seeing ~ 0.85 arcseconds), and benefited from our improved mastering of the new mode (efficiency was four times better than during the first light). A similar instantaneous attenuation was confirmed. To calibrate our detection limits against flux losses induced by PCA, we injected fake companions (at 15σ) prior to PCA and measured their throughput after PCA. We used the derived throughput map to renormalise the initial contrast curve *a posteriori* (Figure 6). This shows excellent detection capabilities down to the IWA of the AGPM. The final calibrated contrast presented here (green dash-dot curve), is limited by the small PA range, especially at small angles. The floor reached beyond an offset of 1-arcsecond is due to the background at *L′*, and will be lower for brighter targets and/or longer integrations.

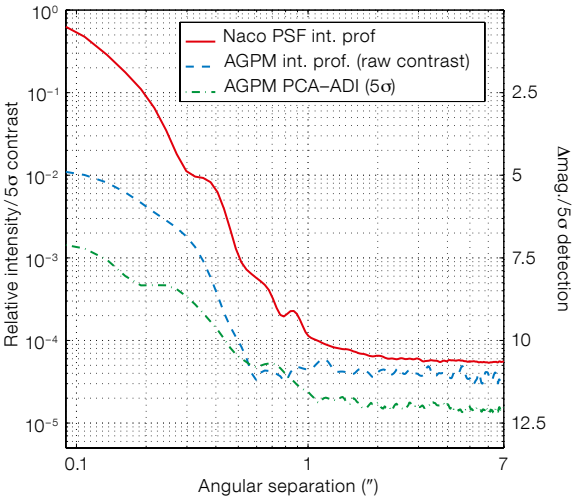

Figure 6. Normalised azimuthally averaged relative intensity profiles and contrast curve on a log–log scale. The plain red curve shows the intensity profile of a typical saturated NACO *L′* PSF (similar brightness and exposure time). The blue dashed curve shows the AGPM intensity profile before PCA, demonstrating the instantaneous contrast gain provided by the coronagraph at all spatial frequencies within the adaptive optics control radius (~ 0.7 arcseconds). The green dash-dot curve presents the reduced PCA–ADI 5σ detectability limits (40 frames, 800 s, ΔPA ≈ 30°), taking both the coronagraph off-axis transmission and the PCA–ADI flux losses into account.

The β Pictoris disc and planet at *L′*-band: a teaser

During the science verification run on 31 January 2013, we imaged the inner regions of β Pictoris down to the previously unexplored projected radius of 1.75 AU with unprecedented point source sensitivity. The ~ 8 Jupiter-mass planet (see Lagrange & Chauvin [2012], and references therein) was imaged with excellent signal-to-noise ratio (see Figure 7), which, combined with the 5-millarcsecond-level astrometric precision enabled by the phase mask (contrary to Lyot coronagraphs, the star is always visible as a residual doughnut), allowed us to derive excellent photometric and astrometric data points (details to appear in a forthcoming paper, Absil et al. [2013], in preparation). The disc was also clearly resolved down to its inner truncation radius (Milli et al. [2013], in preparation).

It is truly a challenge to directly image such a faint debris disc at 3.8 μm, for which both scattered starlight and dust thermal emission are weak. The relatively bright blobs that are visible away from the plane of the disc are remnants of the highly variable background modulated by the adaptive optics system. They are on similar spatial scales to those of the disc and we are currently studying new methods to isolate the astrophysical signal (disc only, including complex shape and warps) from the background residuals.

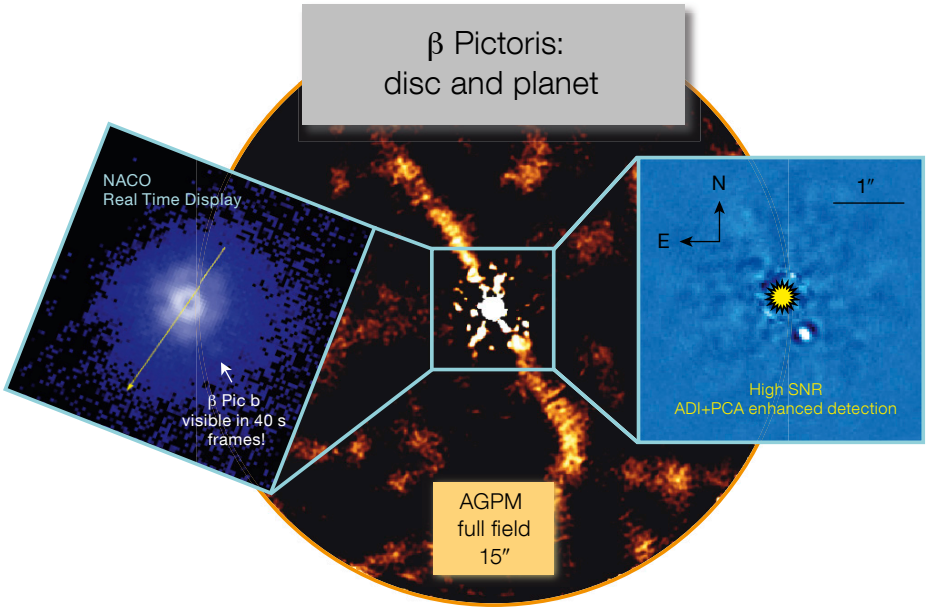

Figure 7. β Pictoris NACO+AGPM *L′*-band observations. This figure showcases the potential of the AGPM over a wide range of spatial scales: the central image represents the full field of view (15 arcseconds) of the AGPM with, at the centre, the masked star surrounded by both the planet (within 0.5 arcseconds) and the faint disc, several arcseconds away. On both sides, the central 4-arcsecond box is zoomed. The left image is a screen capture of the NACO real-time display (in log scale) which shows the star attenuated by the AGPM and the planet visible on single 40-second raw frames (DIT = 0.2 s, NDIT = 100). The right image shows the high signal-to-noise ratio detection of β Pictoris b applying modern post-processing techniques: angular differential imaging (ADI) and principal component analysis. North is up, east to the left.

Outlook

The AGPM was designed to provide exquisite IWA (and OWA) capabilities,

down to 0.9λ/D (0.09 arcseconds at *L′*). The disadvantage of the AGPM's small IWA is its sensitivity to the Strehl ratio (as all coronagraphs) and to pointing errors. The apodising phase plate (APP) is another advanced coronagraph offered at *L′* (see, e.g., Kenworthy et al., 2013). The only, but significant, benefit of this pupil-plane phase apodiser over the AGPM is its intrinsic immunity to tip-tilt errors. This advantage, which has to be traded off against the significantly limited field of view provided by the APP, is decisive when tip-tilt is an issue, as was the case with NACO prior to November 2011 (Girard et al., 2012). However, it is less obvious when the instrument provides nominal PSF stability. In a single technical run, the *L′*-band AGPM has proved to be a reliable coronagraphic solution, and one of the best high-contrast imaging modes of NACO (and most likely worldwide). Combined with ADI, we have demonstrated that high contrast of the order of $\Delta L' > 7.5$ mag can be reached from the IWA of 0.09 arcseconds outwards, even with very modest on-source integration time, PA variation and average conditions. The field of view is a clear 360° discovery space 15 arcseconds in diameter. The coronagraph is optimised for pupil tracking and is easy to use, thanks to the stability of the NACO *L′*-band PSF.

The vortex coronagraph is now the most advanced new generation coronagraph brought to operational level (it is offered at Palomar at *H* and *K*, at *L′* on NACO and at *N* on VISIR). Moreover, it has recently demonstrated 10^{-9} raw contrast capabilities in the visible at NASA's Jet Propulsion Laboratory's high contrast imaging testbed (Mawet et al., 2012). This coronagraphic solution, which is simple, reliable and now quite affordable, is foreseen for future coronagraphic space-based missions dedicated to exoplanet imaging. Last, but not least, it is considered as a potential baseline for the European Extremely Large Telescope high-contrast imagers, at near-infrared (EPICS-PCS), and/or mid-infrared wavelengths (METIS).

References

Beuzit, J.-L. et al. 2010, in *Pathways Towards Habitable Planets*, eds. Coudé du Foresto V., Gelino D. M. & Ribas. I., ASP Conf. Series, 430, 231
Boccaletti, A. et al. 2004, PASP, 116, 1061
Chauvin, G. et al. 2010, A&A, 509, A52
Crepp, J. R. & Johnson, J. A. 2011, ApJ, 733, 126
Delacroix, C. et al. 2013, accepted by A&A
Girard, J. H. V. et al. 2012, Proc. SPIE, 8447
Kasper, M. et al. 2007, A&A, 472, 321
Kenworthy, M. A. et al. 2013, ApJ, 764, 7
Lagrange, A.-M. & Chauvin, G. 2012, The Messenger, 150, 39
Macintosh, B. A. et al. 2012, Proc. SPIE, 8446
Marois, C. et al. 2008, ApJ, 673, 647
Marois, C., Macintosh, B. & Veran, J.-P. 2010, Proc. SPIE, 7736, 52
Martinache, F. et al. 2012, Proc. SPIE, 8447
Mawet, D. et al. 2005, ApJ, 633, 1191
Mawet, D. et al. 2006, A&A, 448, 801
Mawet, D. et al. 2009, Optics Express, 17, 1902
Mawet, D. et al. 2012, Proc. SPIE, 8442
Mawet, D. et al. 2013, A&A, 552, 13
Oppenheimer, B. R. et al. 2013, ApJ, 768, 24
Soummer, R., Pueyo, L. & Larkin, J. 2012, ApJ, 755, L28
Spiegel, D. S. & Burrows, A. 2012, ApJ, 745, 174
Vigan, A. et al. 2012, A&A, 544, A9

Links

[1] telbib: http://www.telbib.eso.org

FORS1 image of the young star-forming region IC 2944, which was released to mark the 15th anniversary of the first light of VLT UT1 on 25 May 1998. The colour image is formed from exposures in three broadband (*BVR*) and two narrowband filters (centred on the emission lines [O III] 5007Å and Hα). The extended emission across the whole image is ionised by hot early-type stars in the cluster and some prominent dust globules are silhouetted against the background H II region. Further details can be found in Release eso1322.